Journal of Materials Chemistry C

ROYAL SOCIETY OF CHEMISTRY

PAPER

View Article Online
View Journal | View Issue

Cite this: J. Mater. Chem. C, 2024, 12, 14944

Electrogelation of PEDOT:PSS and its copolymer for bioelectronics†

Christopher Slaughter,‡[a] Santiago Velasco-Bosom,‡[a] Xudong Tao,[a] Ruben Ruiz-Mateos Serrano,[a] Stefany Kissovsky,[a] Ryo Mizuta,[a] Daniele Mantione,[bc] Scott T. Keene,[ad] George G. Malliaras *[a] and Antonio Dominguez-Alfaro *[a]

Received 9th July 2024,
Accepted 8th August 2024

DOI: 10.1039/d4tc02908a

rsc.li/materials-c

There is strong interest in developing scalable deposition techniques for conducting polymer coatings for applications in bioelectronics. Here, we explore the potential of electrogelation to develop coatings from poly(3,4-ethylenedioxythiophene) polystyrene sulphonate (PEDOT:PSS) and its copolymer with poly (styrene sulphonate-*co*-styrene methanamine) (PEDOT:PSS-*co*-PSMA). The coatings were used to lower the impedance of screen-printed silver electrodes, leading to a decrease in the voltage needed to achieve cutaneous stimulation of small fibres and an increase in the signal-to-noise ratio in cutaneous biopotential recordings. Additionally, PEDOT:PSS-*co*-PSMA was integrated as the gate electrode in an organic electrochemical transistor, showing improved performance compared to non-modified and PEDOT:PSS-coated gold electrodes, *i.e.*, a threshold voltage decreased from 0.7 V for pristine gold to 0.5 V for the PEDOT:PSS-*co*-PSMA gate electrode. The results show that electrogelation offers a scalable and cost-effective solution for the deposition of conducting polymers, including non-solution-processable conducting polymers, as performance-enhancing coatings for bioelectronic applications.

1. Introduction

Electropolymerisation is one of the most effective techniques for the formation of controlled conducting coatings on complex substrates, such as microwires and micropillars, where spin coating is not a viable option.[1] Of all conducting polymers, poly(3,4-ethylenedioxythiophene) (PEDOT) doped with polystyrene sulphonate (PSS) is considered a gold standard material for bioelectronics because it reduces impedance at the skin–electrode interface, leading to a significant enhancement of the signal-to-noise ratio and the overall sensitivity of the device.[2] Since PSS is a water-soluble polyelectrolyte, electropolymerisation of PEDOT:PSS is typically restricted to using water as the solvent. However, EDOT monomers present poor solubility in water (below 10 mM) and their oxidation potential is over 1.2 V *vs.* Ag/AgCl, which exceeds the electrochemical window of water. Electropolymerisation on small electrodes is particularly challenging as they possess high impedance and limit the polymerisation currents. As an example, Cramer *et al.*[3] polymerised PEDOT:PSS on electrodes of 50 μm in diameter. They used a galvanostatic protocol with a controlled current density of 2 mA cm^{-2} and a monomer concentration of 10 mM EDOT. In addition, Montes *et al.*[4] selectively electropolymerised PEDOT:PSS on the tip of gold-coated structures of 10 μm using cyclic voltammetry below 1 V. Due to the limited electrochemical window and solubility of EDOT, most of the examples presented in the literature perform electropolymerisation in organic solvents that exhibit intrinsically wider electrochemical windows and soluble electrolytes. As a result, common conducting coatings consist of PEDOT doped with perchlorates (PEDOT:ClO_4), tetrafluoroborates (PEDOT:BF_4), or hexafluorophosphates (PEDOT:PF_6), among other examples.[5–8]

In addition, the electropolymerisation of PEDOT exhibits limited compatibility with non-noble metals such as tungsten and copper as well as with metallic inks (*e.g.*, silver and graphite) employed in screen-printed devices. This is because the metal in these electrodes undergo oxidation and solubilisation into the electrolyte before the EDOT monomers reach their polymerisation potential *c.a.* 1.2 V *vs.* Ag/AgCl. One way to overcome this limitation is to generate a layer of oxide through annealing that improves the nucleation of the conducting

[a] Electrical Engineering Division, Department of Engineering, University of Cambridge, 9 JJ Thomson Ave, Cambridge, CB3 0FA, UK. E-mail: gm603@cam.ac.uk, ad2151@cam.ac.uk
[b] POLYMAT, University of the Basque Country UPV/EHU, Avenida Tolosa 72, Donostia-San Sebastián, Gipuzkoa 20018, Spain
[c] IKERBASQUE, Basque Foundation for Science, 48009, Bilbao, Spain
[d] Cavendish Laboratory, University of Cambridge, JJ Thomson Ave, Cambridge, CB3 0H, UK

† Electronic supplementary information (ESI) available. See DOI: https://doi.org/10.1039/d4tc02908a

‡ Authors contributed equally to this work.

polymer and avoids metal degradation.[9] However, this type of modification is incompatible with most electrode types due to their sensitivity to heat and the inability of non-oxidizable noble metals, such as gold and platinum, to form stable oxide layers. These restrictions pose a significant challenge for extending the applicability of PEDOT-based electrode fabrication beyond noble metal substrates.

Electrochemical gelation (electrogelation) is a versatile technique for the coating of all types of metals, especially those prone to oxidation, such as copper, aluminium, iron, lead or magnesium. It was first described for silk fibroin by Kaplan and co-workers, using a high voltage (25 V) in a two-electrode electrochemical cell.[10] The formation of a silk-based gel involves water electrolysis, which decreases the local pH of the aqueous silk fibroin solution, driving conformational changes and a sol–gel transition of the protein.[11] Feig *et al.*[12] demonstrated electrogelation of PEDOT:PSS on copper electrodes as a sacrificial layer. In this electrogelation process, copper is oxidized at 0.5 V, generating Cu^{2+} ions, which dissolve in PEDOT:PSS, increasing the viscosity of the solution near the electrode and forming a hydrogel clearly defined within the boundary of the Cu layer. Besides Cu^{2+}, PEDOT:PSS has also been shown to gelate in solution or change its mechanical properties[13] when monovalent cations such as lithium (Li^{+})[14] as well as multivalent cation salts such as aluminium (Al^{3+}),[15] magnesium (Mg^{2+}),[16] ionic liquids,[17,18] and deep eutectic solvents[19] are added.

Some examples in the literature have used electrogelation to create conducting hydrogel-based devices for biosensing. Liang *et al.* used PEDOT:PSS electrogelation to coat etched gold microwires (m-Au) and carbon nanotube fibres (CNTf).[20,21] In the first case, the modified gold surface was coated with copper, followed by the deposition of PEDOT:PSS through electrogelation. Au/Cu/PEDOT:PSS microwires were used for electrochemical amperometric sensing of H_2O_2, glucose, dopamine (DA) and levodopa (L-Dopa) with good sensitivity and limit of detection. In the second example, glucose oxidase (GOx) was adsorbed on the surface of CNTf/Cu microwires for manufacturing third-generation glucose biosensors by using PEDOT:PSS conducting hydrogels. The sensitivity of the biosensor was improved from 198 μA cm^{-2} mM^{-1} to 44 μA cm^{-2} mM^{-1} thanks to the direct electron transfer mechanism between the conducting hydrogel and GOx. Electrogelation has also been used for the formation of a MXene hydrogel (Ti_3C_2) and a Ti_3C_2/PEDOT:PSS hydrogel composite. Ti_3C_2 sheets in suspension are negatively charged due to the –OH/–F terminals, and the gelation can be induced by the addition of metal cations.[22] The MXene-hydrogel demonstrated good energy storage devices with a capacitance of 33.3 mF cm^{-2} and prominent current responses towards metabolites (sensitivity of H_2O_2: 166 μA mm^{-1} cm^{-2}; sensitivity of DA: 212 nA μm^{-1} cm^{-2}). Furthermore, the PEDOT:PSS/Ti_3C_2 hydrogel was utilised for a high-resolution pressure sensor microarray, with a particular focus on recognizing tactile stimuli and identifying Braille letters.[23,24] Other composites that combine reduced graphene oxide (rGO) and electrogelated PEDOT:PSS were employed as bioelectronic test strip patches. These were fabricated by the electrogelation of PEDOT:PSS/rGO on interdigitated electrodes of Au/Cu for glucose sensing.[25] These studies established electrogelation as a promising method for applying conductive coatings to surfaces with complex geometries on small, medium, and large scales on a variety of electrodes.

Here, we use electrogelation of PEDOT:PSS on blade-coated silver electrodes as a lithography-free technique for the development of bioelectronic devices. We have fabricated a set of devices for small fibre stimulation and electromyography (EMG) recording. Finally, we have explored the use of the electrogelated PEDOT:PSS-copolymer as a gate electrode in organic electrochemical transistors (OECTs) to decrease the threshold voltage from 0.7 V for pristine gold to 0.5 V for the PEDOT:PSS-copolymer. Additionally, we describe the use of electrogelation as an alternative deposition method for PSS copolymer dopants which prevents the formation of aggregates and inhomogeneous coatings caused by drop- or spin-coating.

Antonio Dominguez-Alfaro

Antonio Dominguez-Alfaro is a multidisciplinary scientist working at the interface between chemistry, engineering, manufacturing, and biology. He obtained his BSc and MSc degrees in Chemical and Industrial Engineering from the University of Huelva and completed his PhD degree in Applied Chemistry at the University of the Basque Country in 2021 under the supervision of Prof. David Mecerreyes and Prof. Maurizio Prato. He started his post-doctoral research at CIC biomaGUNE with Prof. Aitziber Cortajarena, focusing on the synthesis of conducting protein hybrids. Later, he moved to the University of Cambridge (UCAM) as a Margarita Salas fellow to work with Prof. George G. Malliaras. Since October 2023, he has been a Research Associate at UCAM interested in changing the paradigms of the fabrication of devices, in particular for bioelectronics, using a material chemistry approach.

2. Results and discussion

In this work, we focused on the manufacturing of three types of electrodes where electrogelation of PEDOT:PSS presents fundamental advantages: electrodes for stimulation, biopotential recording, and gate electrodes in OECTs. The electrodes and tracks were fabricated by depositing silver nanoparticle paste on various flexible substrates by means of the blade-coating process previously described.[26–28] Fig. 1 illustrates the fabrication process, which can be described as follows: (1) silver (Ag) nanoparticle ink is applied by blade-coating onto laser-cut silicon-based tape employed as a mask with the desired shape; (2) copper (Cu) is electroplated onto the silver-coated electrodes

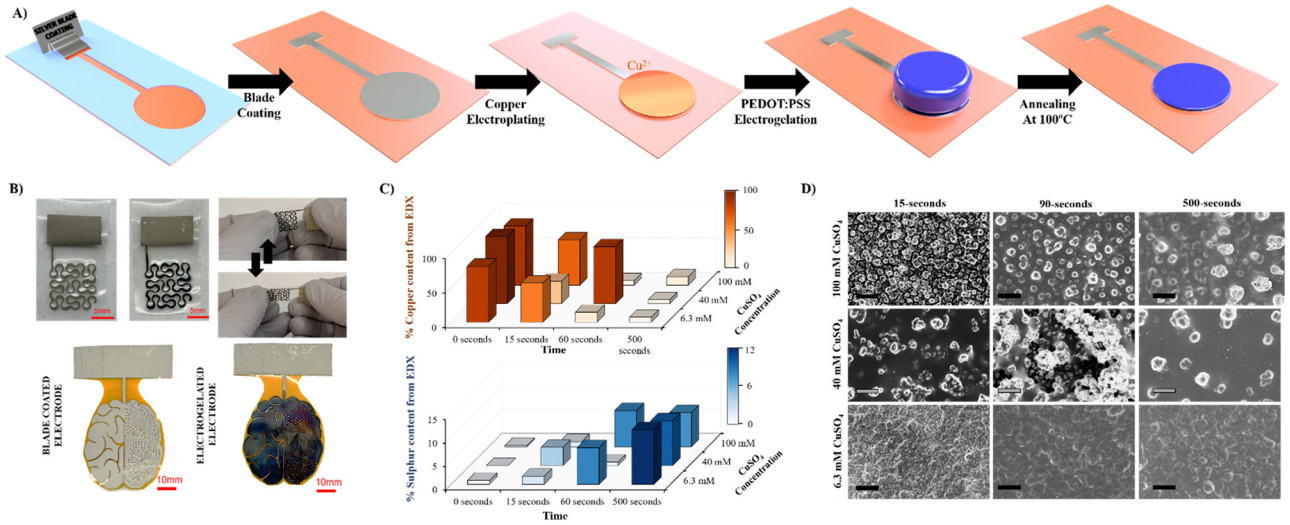

Fig. 1 (A) Electrode manufacturing process. The silver nanoparticle paste is blade coated on the substrate (*e.g.*, Kapton substrate) using a silicon-based tape mask, copper is electroplated on the silver electrode, the electrode is immersed in 10 v/v% PEDOT:PSS dilution and the copper is oxidized at 0.5 V forming a gel. Finally, the gel is collapsed *via* annealing for 5 min at 100 °C. (B) Examples of electrodes bladed coated (grey) with silver ink and after electrogelation (blue) on polyurethane (top) and Kapton (bottom). (C) Bar graph of the EDX elemental analysis of electrodes electrogelated at different times and under different copper salt conditions; orange for the percentage of copper and blue for the percentage of sulphur. (D) SEM morphologies for different electrogelation times and copper electroplating concentrations.

(Ag/Cu) at a constant voltage of 1.5 V using a two-electrode configuration (Ag *vs.* Cu). In this step, copper sulphate ($CuSO_4$) is used as the supporting electrolyte; (3) the Ag/Cu electrode is electrochemically oxidised at 0.5 V, generating Cu^{+2} salt in the presence of a diluted (9 : 1) PEDOT:PSS solution as the supporting electrolyte, producing a hydrogel on the surface of the electrode. A three-electrode configuration is employed for this step where Ag/Cu serves as the working electrode, platinum as the counter electrode and Ag/AgCl as the reference electrode; (4) finally, the Ag/Cu/PEDOT:PSS hydrogel is gently washed with DI water and annealed at 100 °C. Fig. S1 (ESI†) illustrates the fabrication process in detail. The combination of electrogelation with blade coating allows the manufacturing of complex geometries such as fractals or electronic circuitry resembling a brain, on top of different types of substrates, such as stretchable polyurethane (PU), glass, and Kapton© polyimide (Fig. 1B). Furthermore, it offers an alternative method to the traditional metal sputtering process for the fabrication of stretchable and conductive electrodes, as reported in the literature.[29]

Copper was selected as a sacrificial metal due to its oxidation to copper salt (Cu^{2+}), which occurs at low potentials (*ca.* 0.5 V *vs.* Ag/AgCl at acid pH), below the electrochemical window of water.[30] Feig and co-workers reported oxygen evolution reactions during the electrogelation process for higher dilutions of PEDOT:PSS than 10 v/v%.[12] For these PEDOT:PSS concentrations, the electrolyte forms larger double electrolyte resistance on the working electrode, thus demanding larger voltages during galvanostatic reactions. This effect causes oxygen evolution reactions, which are incompatible with device patterning, since the gas generated delaminates the electrode considerably. Based on this, we set the optimal PEDOT:PSS concentration for electrogelation to be 10 v/v% and decided to control the formation of the PEDOT:PSS hydrogel by using different copper electroplating coatings, *i.e.*, 6.4, 40 and 100 mM of $CuSO_4$. However, it is worth mentioning that similar to the observation by Feig *et al.*, the use of galvanostatic electroplating (−3 mA) across all electroplating conditions introduced variability in electrolyte resistance. At lower electrolyte concentrations, the current was insufficient to obtain the necessary potential for homogeneous copper deposition. Consequently, to ensure successful coating across all copper salt concentrations, electroplating was conducted using a constant voltage of 1.5 V for 20 minutes. Silver was also tested as the sacrificial layer for the gelation of PEDOT:PSS; however, the silver salts did not form gels, probably due to weaker coordination effects between Ag^+ and PSS^-. Fig. 1C shows a bar graph with three copper and sulphur compositions analysed by SEM-EDX of the three electroplated depositions (0 seconds) and their corresponding electrogelation times (15, 90 and 500 seconds). Moreover, Table S1 and Fig. S2 (ESI†) shows all the values used for the bar graph and the plots of 6.3 mM copper electroplated and 15, 90 and 500 s PEDOT:PSS electrogelation times. As expected, copper is mostly present under the three electroplating conditions with 81.2 ± 16.0, 97.3 ± 2.9 and 85.9 ± 4.0% for 6.3, 40 and 100 mM $CuSO_4$, respectively. The electroplating of copper produces particle-like structures similar to the silver blade coated electrodes for 6.3 mM Ag/Cu electrodes, *i.e.* 0.8 ± 0.2 μm for 6.3 mM Ag/Cu electrodes and 0.9 ± 0.3 for Ag electrodes. As the concentration of $CuSO_4$ increases, there is a corresponding augmentation in particle dimensions. Specifically, particle sizes measure 1.5 ± 0.4 μm and 2.1 ± 0.7 μm at copper salt concentrations of 40 mM and 100 mM, respectively. Fig. S3 (ESI†) shows that the size of the

particles is in line with the increase in the concentration of copper salt.[28] When the electrodes are electrogelated, the amount of sulphur increases proportionally to the reaction time, reaching the maximum at 500 seconds of electrogelation with 11.7 ± 1.5, 9.5 ± 0.7 and 7.3 ± 0.8% for 6.3, 40 and 100 mM $CuSO_4$, respectively (see Fig. 1C). In Fig. 1D, the morphology of the electrodes after electrogelation is shown. For longer electrogelation times, the coating on the electrode is more uniform and thicker. Similarly, the particle size also increases with electrogelation time (refer to Table S2, ESI†). Despite the morphology under lower copper concentration conditions (6.4 and 40 mM $CuSO_4$) and 15-seconds electrogelation, there is a slight increase in particle size, from 0.8 ± 0.2 and 1.5 ± 0.4 μm for 6.3 and 40 mM $CuSO_4$ to 1.9 ± 0.4 and 1.9 ± 0.9 μm, respectively. We hypothesize that when electrogelation is performed for short times, the copper consumption is limited by diffusion near the shell, creating flat regions decorated with microparticles as illustrated in Fig. 2A. This effect is observable for the two conditions for which the density of copper microparticles is low *i.e.* 6.3 and 40 mM $CuSO_4$. AFM was performed to compare the roughness and morphology of Ag, Ag/Cu and Ag/Cu/PEDOT:PSS electrodes at 6.3 mM of $CuSO_4$ and 15-seconds of electrogelation (Fig. 2B–D). In agreement with our observation, the root mean square (RMS) roughness was lower for Ag/Cu/PEDOT:PSS than that for other samples, where the RMS roughness was 148.0, 227.8 and 81.5 for Ag, Ag/Cu, Ag/Cu/PEDOT:PSS electrodes, respectively.

2.1. Small fibre stimulation

Our group has recently reported a lithography-based manufacturing process for flexible interdigitated electrodes (FIDE) made of gold metal coated with PEDOT:PSS. The FIDE electrodes were designed for the stimulation of small fibers on the forearm in humans by using charge current injection pulses. The fabrication process consisted of six subsequent steps that comprised the following: a 2 μm layer of Parylene-C (PaC) deposition, then spin-coating a layer of poly-dimethylsiloxane (PDMS) on top of it before depositing a second 2 μm layer of PaC. Subsequently, the deposition of metal tracks, followed by spin coating and etching of PEDOT:PSS. Thanks to the combination of PEDOT:PSS electrogelation and blade coated silver electrodes, we were able to simplify and therefore speed up the process with similar results.[31]

Three different coatings for FIDE devices were used to compare the effects of the coatings in the stimulation of small muscle fibres in humans, the FIDE of plain silver (Ag), the chlorine coated silver FIDE (Ag/AgCl), and the electrogelated PEDOT:PSS coated FIDE (Ag/Cu/PEDOT:PSS) (Fig. 3A). Ag/AgCl FIDEs were used as control electrodes, due to their lower impedance on the skin, which improved the stimulation efficiency.[32] PEDOT:PSS was electrogelated under the lowest copper conditions (6.3 mM $CuSO_4$) and the shortest electrogelation time (15-s) to avoid electrical shorting between electrodes. The interelectrode distance (150 μm) presented a significant challenge in selectively depositing copper and PEDOT:PSS. During electrochemical reactions, the material grows and tends to form interconnected paths between different electrode fingers. This effect occurs when the copper concentration is high, leading to the formation of dendrites of copper, or when the PEDOT:PSS electrogelation process exceeds 15 seconds, allowing copper diffusion to facilitate gel formation over the whole surface, forming a single electrode. To verify the presence and uniformity of the PEDOT:PSS layer on the electrodes, EDX was used. In this case, one device was partially submerged during electrogelation, coating only some of the finger electrodes while leaving the copper platting exposed in the rest. Fig. 3B shows the interface between the two different areas analysed *i.e.* coated (top) and non-coated (bottom). Moreover, on the left side of Fig. 3B, the SEM image is combined with the EDX scanned area. The EDX scanned area reveals the presence of elements such as silver, carbon, copper, sulphur, and oxygen. Additionally, on the right side of the figure, the sulphur element mapping measured by EDX is displayed along with a plot showing the sulphur count obtained. The sulphur content averaged at 60 counts for PEDOT:PSS-uncoated areas, whereas a three-fold increase is observed for fingers coated with PEDOT:PSS, reaching total values of up to 180 counts. This result confirms that the coating is selective and successful for these given electrogelation parameters.

Additionally, we evaluated the consequence of coating the FIDEs with this material against the skin impedance. Electrochemical impedance spectroscopy (EIS) was performed. As expected, the use of conducting electrogelated coatings reduces the electrode impedance by an order of magnitude from 2082 ± 3300 to 263 ± 157 kΩ for Ag electrodes and Ag/Cu/15-s PEDOT:PSS, respectively (Fig. S4, ESI†).

Subsequently, the three different coatings were analysed for the selective stimulation of small fibres in humans. Most medical

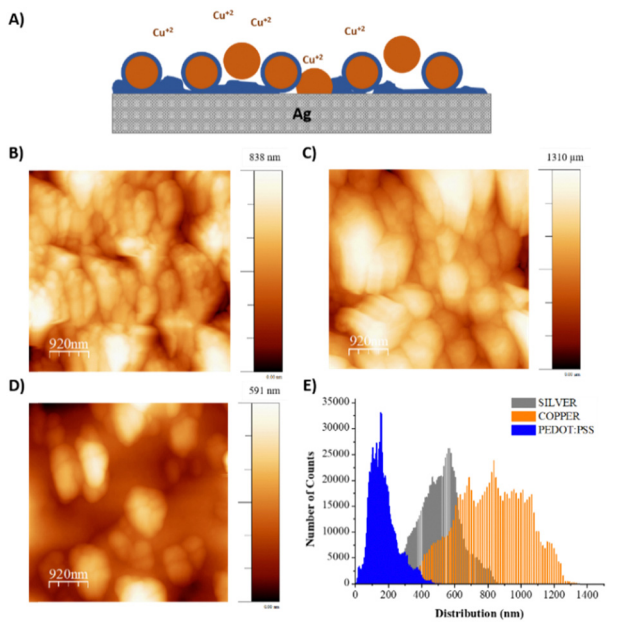

Fig. 2 (A) Diagram describing the behaviour of PEDOT:PSS electrogelation at low copper concentrations (6.3 and 40 mM of $CuSO_4$). AFM images of the (B) Ag electrode, (C) Ag/Cu electrode using 6.3 mM $CuSO_4$ and (D) Ag/Cu/15-s PEDOT:PSS electrode. (E) The root mean square (RMS) roughness of the three electrodes.

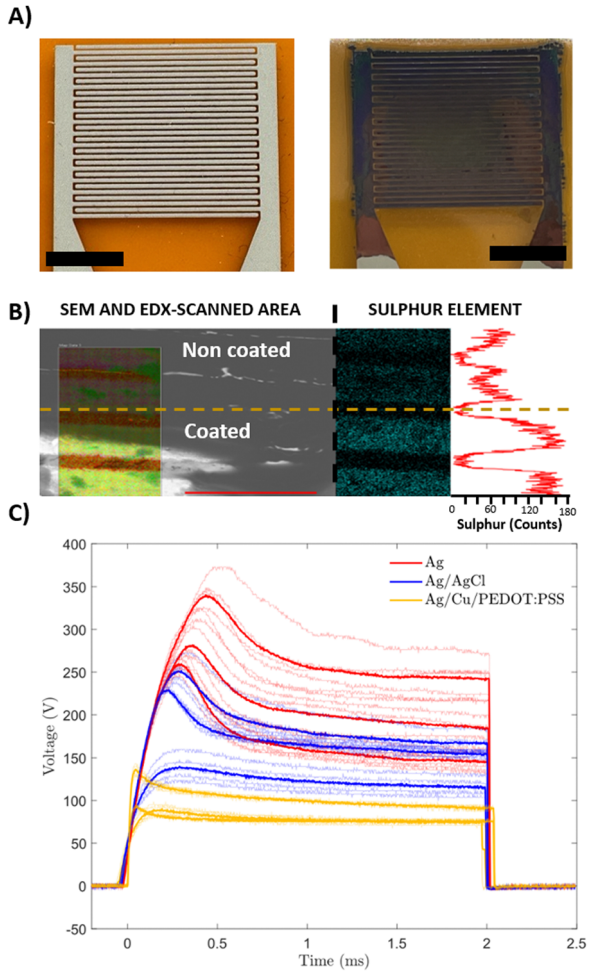

Fig. 3 (A) Optical images of pristine and PEDOT:PSS coated FIDEs (scale bar: 4 mm). (B) SEM-EDX spectroscopy of FIDE fingers. The top two fingers were not coated with PEDOT:PSS, observing a lower sulphur count, compared to the bottom fingers, coated with PEDOT:PSS where a greater count number is appreciated. (C) Voltage applied to inject a current of 1.3 mA using 2 ms pulses. Three Ag/AgCl devices (blue) and three silver (red) and three Ag/Cu/PEDOT:PSS (gold) electrodes are compared. Thick tracks correspond to the average of each device, while thin traces correspond to each individual stimulation.

equipment limits the maximum stimulation voltage for safety purposes, and therefore, higher stimulation voltages might saturate the device possibilities, limiting the physician's diagnostic capabilities, as the range of currents induced is narrower. Fig. 3C shows the voltage stimulation for each coated electrode. It is worth mentioning that the term "overshoot" or "overshoot ratio" refers to the difference between the maximum peak voltage and the plateau voltage. An initial overshoot during the first second and stabilisation on a plateau at the end of the stimulation pulse is observed for all the cases. Because of the reduced skin impedance, both coatings (Ag/Cl and PEDOT:PSS) reduce the voltage required to produce the stimulation compared to the plain Ag electrodes. In the case of the AgCl-coated electrodes, they required an average of 50 V less in the ending plateau, showing voltage values in the order of 145 V, compared to the plain Ag electrodes that plateau around 195 V. The effect observed for Ag/Cu/PEDOT:PSS electrogelated devices was more pronounced, recording average voltages at a plateau of 85 V. When comparing the overshooting phenomena observed at the beginning of the stimulating pulse, all the electrodes show a similar overshoot ratio (maximum peak compared to plateau voltage), 139% for AgCl coating devices, 130% for Cu/PEDOT:PSS coated electrodes and 146% for plain silver devices on average. In addition, the Ag/Cu/PEDOT:PSS electrode stimulation signals stabilised around 115 V, whereas Ag/AgCl devices required 30 extra volts to reach the stabilisation plateau. Furthermore, it was observed that the maximum overshooting peaks in PEDOT:PSS electrogelated devices were consistently lower in absolute values compared to those recorded with AgCl-coated electrodes. Among the three coatings tested, Ag/Cu/PEDOT:PSS coated electrodes demonstrated superior performance, reducing the voltage and amplitude overshooting obtained, thus demonstrating great potential for single fibre stimulation.

2.2. Body surface potential mappings (BSPMs)

In addition to the use of lithography-free conducting coatings for stimulation, our group has recently investigated the potential of using ionic liquids (ILs) as additives to PEDOT:PSS to reduce the skin impedance and enhance the recording of muscle activation in the forearm using body surface potential mappings (BSPMs).[26] The performance of the array enabled high-quality spatiotemporal recordings of EMG that allow discrimination of individual finger motions. While the fabrication process was already lithography-free, the deposition of the PEDOT:PSS/IL gel was carried out *via* drop casting, which led to issues such as gel-leaking. In this section, we used electrogelation to selectively deposit PEDOT:PSS on blade-coated Ag devices, improving the performance of the BSPM and finger classification.

Fig. 4A shows the appearance of non-coated Ag arrays and coated Ag/Cu/PEDOT:PSS arrays. The electrodes were fabricated on Kapton with silver blade-coating, followed by copper plating and PEDOT:PSS electrogelation for 500 seconds. The array was then left to anneal at 100 °C for 5 minutes until the gel collapses, forming a controlled coating. Unlike FIDEs, the inter-electrode distance was designed to be larger, 3 mm *vs.* 150 μm. Therefore, larger electrogelation times were allowed, increasing the thickness and protrusion of the electrodes. Across the 4 types of fabricated arrays (6.3 mM, 40 mM, and 100 mM $CuSO_4$ copper plated with an Ag electrode array), electrochemical impedance spectroscopy (EIS) measurements were taken from 100 kHz down to 1 Hz as shown in Fig. 4B. At 50 Hz, the EIS of Ag electrodes was similar to different longer PEDOT:PSS electroplated electrodes (500-s), *i.e.* 2.08 ± 3.30, 0.82 ± 0.25, 1.09 ± 0.16, and 0.86 ± 0.14 MΩ for 6.3 mM, 40 mM, and 100 mM $CuSO_4$, respectively. These values are in the same range to the PEDOT:PSS/ILs previously mentioned electrodes with 2.7 MΩ at 60 Hz.

The arrays were placed on the back of a volunteer's forearm. Subsequently, activation–relaxation experiments on the forearm were performed. Firstly, 10 seconds of baseline were

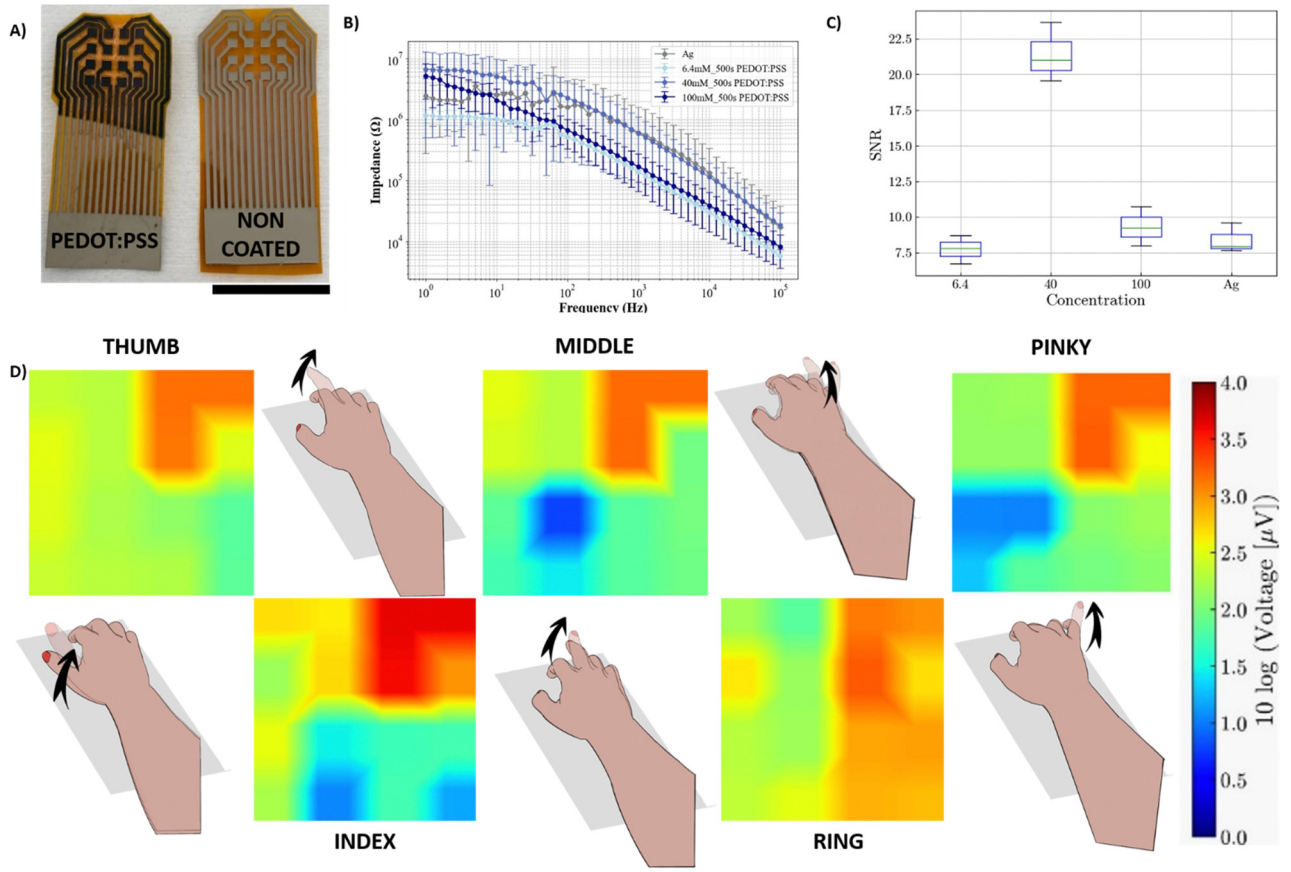

Fig. 4 (A) Photographs of the BSPM electrodes coated (left) and non-coated (right) with PEDOT:PSS using 6.3 mM $CuSO_4$ and 500-s electrogelation (scale bar: 2 cm). (B) EIS on the skin with 6.3, 40 and 100 mM of $CuSO_4$ and 500-s electrogelation. (C) Signal-to-noise ratio (SNR) of the three BSPM electrodes on the forearm during individual finger contraction. (D) Heat map of the SNR across electrode array channels for each individual finger extension. Representative diagrams of each motion are included.

recorded, followed by intervals of 5 s of muscle activation, during which participants were asked to raise each finger (thumb, index, middle, ring, and little) five times, followed by 5 s of rest. The signal-to-noise-ratio (SNR) is displayed in Fig. 4C, where the three electrogelated BSPM electrode arrays are compared with the non-coated silver electrode array. We observe similar SNR values for the non-coated Ag array and the 6.3 mM $CuSO_4$ electrogelated array with values of 8.41 ± 0.84 and 7.75 ± 0.8, respectively, whereas the 40 mM and 100 mM $CuSO_4$ electrogelated arrays show increases in the SNR, with 21.41 ± 1.69 and 9.33 ± 1.12, respectively. This suggests the existence of optimum concentrations of $CuSO_4$ in the electrochemical copper plating process that can lead to more efficient PEDOT:PSS coatings during the electrogelation process, substantially improving the SNR. Finally, the electrophysiological activity because of each finger movement is displayed in Fig. 4D for each individual finger. The arrays enable the non-invasive spatial and temporal mappings of the progression of polarization and depolarization waves in the muscle fibres across the forearm. In comparison to the Ag electrodes without electrogelated PEDOT:PSS, it can be observed that the electrogelated Ag/Cu/PEDOT:PSS arrays display a superior SNR across the channels of the array which can be attributed to the lower electrode-skin impedance facilitated by the PEDOT:PSS layer. The mappings of the polarisation and depolarisation of the underlying muscle fibres are visualised using a heat map that represents the polarity and intensity of these waves. Moreover, the electrogelated array's higher signal-to-noise ratio enables significantly higher-resolution imaging of recordings compared to basic silver electrode arrays. In conclusion, electrogelated PEDOT:PSS arrays can be utilized in clinical settings to understand the performance of specific muscle group activities.

2.3. PEDOT:PSS-copolymer electrogelation

OECTs consist of a PEDOT:PSS channel material separated from the metal or the polymer gate using an electrolyte. Upon the application of a gate voltage, ions from the electrolyte are injected into the channel, de-doping and changing its conductivity. One of the key parameters of OECTs is the threshold voltage (Vth), which determines the point at which the channel between the source and drain electrodes starts to conduct. Tuning Vth can improve the amplification properties at lower voltages.[32] Recently, Vth has been tuned through the use of polymer-doped gates, controlling the electrochemical potential

at the gate electrode and by spin coating poly(vinyl phosphonic acid-*co*-acrylic acid) on the gate.[33–35]

On the other hand, PEDOT:PSS is a highly π-conjugated material, which allows outstanding and controlled deposition by spin coating. In particular, aliphatic amines have been reported to play a role in doping processes of PEDOT:PSS, following a mechanism with a dual role, *i.e.*, both an electron donor and a proton acceptor.[36,37] However, the addition of a functional group that differs from PSS results in particulate-like depositions, which are detrimental to the performance of the film. Hence, electrogelation was utilized to coat homogeneously gate electrodes with a novel PEDOT:PSS-copolymer that could not be processed using conventional casting methods.

Firstly, a new copolymer of poly (styrene sulphonate-*co*-styrene methanamine) (PSS-*co*-PSMA) (M_w: 32 kDa; $Đ$: 2.1) was synthesised and polymerised in the presence of EDOT by chemical oxidative polymerisation to form a dispersion of PEDOT doped with PSS-*co*-PSMA (Fig. 5A). The result was a blueish dispersion with a similar appearance to PEDOT:PSS, but less colloidally stable in the long term. This is due to the acid pH of the final dispersion; we can assume that the amine of PSS-*co*-PSMA is protonated, hindering the stabilisation of positively charged PEDOT chains. DLS showed a monomodal particle size distribution with a band centred at 242.3 ± 0.2 nm. Fig. 5B shows the electrogelation reaction in the presence of a 10% PEDOT:PSS-*co*-PSMA dispersion on 6.3 mM $CuSO_4$ electrodes at a constant voltage of 0.5 V for 500 seconds. The plot illustrates the decrease of the current as the amount of copper is consumed. SEM-EDX of Ag/Cu/PEDOT:PSS-*co*-PSMA resulted in a composition of 40.3 ± 8.0, 1.6 ± 0.4, and 1.1 ± 0.4% for copper, sulphur, and nitrogen, respectively (Fig. 5C). Moreover, the composition is homogeneous throughout the whole electrode, a major improvement from the PEDOT:PSS-*co*-PSMA deposited by spin coating (Fig. 5D). SEM shows a uniform morphology coated by spherical particles of 1.0 ± 0.2 μm, smaller than its homologous PEDOT:PSS electrogelation (Fig. 5E). Fig. 6A shows a standard OECT configuration as mentioned previously. The coated PEDOT:PSS-copolymer gate electrode was evaluated and its performance was compared with electrogelated PEDOT:PSS and bare gold. The use of electrogelated Ag/Cu/PEDOT:PSS-*co*-PSMA gates causes a shift in the transfer characteristics to lower gate voltages and thus, shifts *V*th to lower potentials compared to the bare gold electrode, as shown in Fig. 6A and B, and to the control Ag/Cu/PEDOT:PSS electrode as shown in Fig. S6 (ESI†).

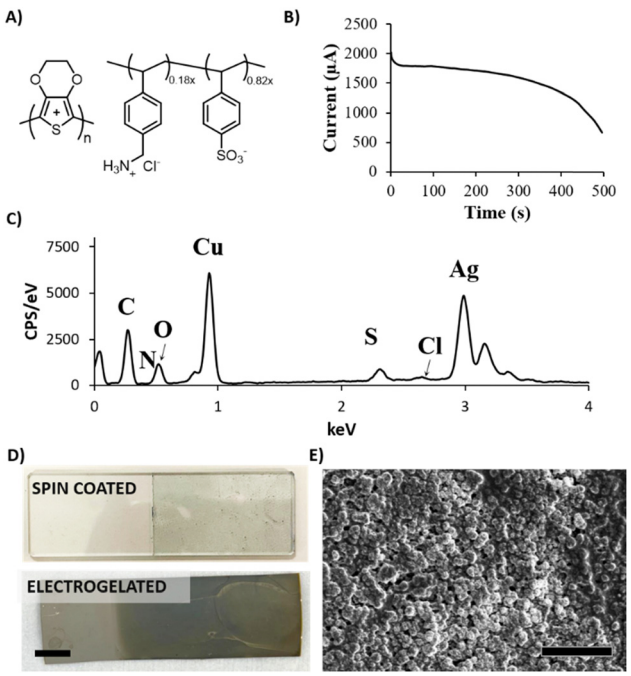

Fig. 5 (A) The chemical structure of PEDOT:PSS-*co*-PSMA. (B) Chronoamperometry of electrogelation for 500 s using 6.3 mM electroplated electrodes. (C) SEM-EDX image of the sample, indicating the presence of the elements. (D) Comparative photographs of PEDOT:PSS-*co*-PSMA spin coated (top) and 500-s electrogelated electrodes (bottom) (scale bar: 1 cm). (E) SEM image of Ag/Cu/PEDOT:PSS-*co*-PSMA electrodes (scale bar: 10 μm).

*V*th was extracted from the transfer characteristics by finding the derivative of the drain current as a function of the gate voltage and extracting the slope in the linear region. A drain voltage of −0.1 V was chosen for the extraction so that the non-uniform doping effects can be minimised as explained by M. Berggren and co-workers.[35] The results showed that *V*th was found to be the minimum for the amine-enriched gate, improving from 0.7 V for the bare gold gate and 0.6 V for the Ag/Cu/PEDOT:PSS control to 0.5 V for Ag/Cu/PEDOT:PSS-*co*-PSMA. The electrogelated Ag/Cu/PEDOT:PSS-*co*-PSMA electrode at a gate voltage of −100 mV required lower currents (6 μA), compared to 40 μA for the bare gold gate and 16 μA for the Ag/Cu/PEDOT:PSS electrode, highlighting the ability of the Ag/Cu/PEDOT:PSS-*co*-PSMA electrode to switch the OECT off at lower gate voltages. Additionally, at the same gate voltage, transconductance bands were also shifted towards lower voltages *i.e.*, 0.31, 0.24 and 0.17 V for gold, electrogelated PEDOT:PSS and electrogelated PEDOT:PSS-*co*-PSMA, respectively. In conclusion to this section, we have first demonstrated that electrogelated Ag/Cu/PEDOT:PSS-*co*-PSMA gates can be used to decrease *V*th and the "OFF" voltage of the OECT compared to the same channel with a standard gold electrode or the PEDOT:PSS coated gate, providing better performance at lower gate voltages. This result showcases the use of electrogelation as an alternative technique to deposit PEDOT:PSS-copolymers with a higher degree of chemical complexity.

3. Experimental

3.1. Materials

All chemicals were used without any further purification. Poly(3,4-ethylenedioxythiophene):poly(styrene sulphonate) (PEDOT:PSS) (PH1000, Heraeus Clevios), silver nanoparticle paste (LS-453-6B, Asahi Chemical Research Laboratory Ltd, Japan), polyimide (Kapton) substrates (DuPont; type HN, 125 mm), and glass slides (CLARITY MICROSCOPE SLIDES; 76 × 55 × 1 mm) were used. Sodium 4-vinylbenzenesulphonate technical, ≥90%,

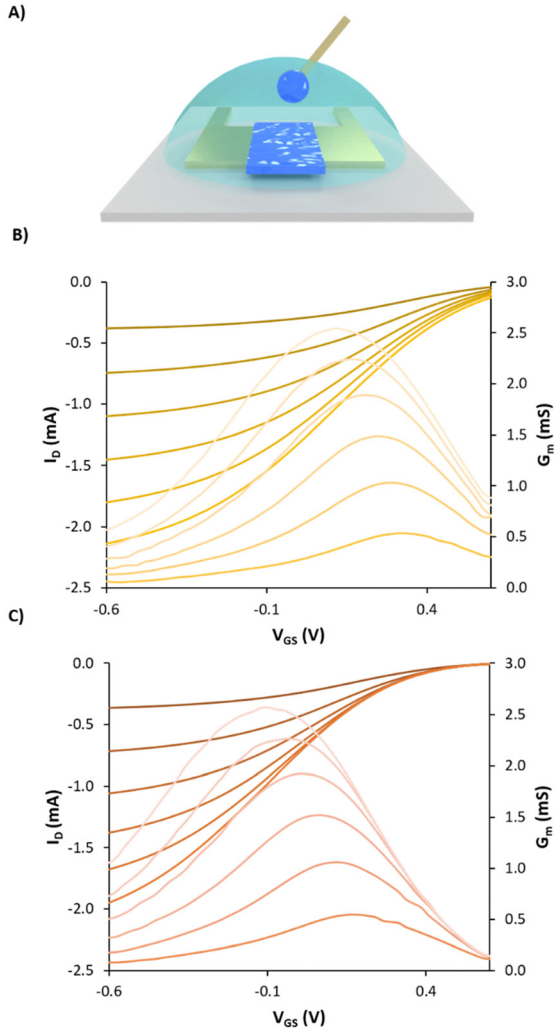

Fig. 6 (A) A schematic representation of an OECT; PEDOT:PSS is deposited on the channel between the drain and the source while the electrogelated Ag/Cu/PEDOT:PSS-*co*-PSMA is used as the gate electrode. Transfer characteristic and transconductance curves at varying drain voltages from 0 to -0.6 V of OECTs with a channel of L = 600 μm and W = 70 μm of the (B) bare gold gate and (C) Ag/Cu/PEDOT:PSS-*co*-PSMA gate. For all cases, R = 2 mm and V_D is set from −0.1 to −0.6 V with an interval of 0.1 V.

2,2′-azobis(2-methylpropionitrile) and D_2O 99.8 atom % D were provided by Sigma Aldrich. (4-Vinylphenyl) methanamine hydrochloride 98% was provided by BLDpharm. Methanol was provided by Fisher Scientific. MilliQ water was prepared using a Millipore A10 system. The dialysis modified cellulose tube membrane was provided by Sigma Aldrich with a MWCO of 14 kDa.

3.2. Substrate preparation

Polyimide (Kapton) substrates were prepared by cutting into 75 mm × 75 mm, the surface was cleaned using a pressurized air gun, and finally washed thoroughly with propan-2-ol ≥ 99.8% (IPA). Afterwards, the Kapton sheets were positioned atop a custom cut steel sheet for silver blade coating. Glass slides (Clarity Microscope Slides C369) of 76 × 56 mm were prepared in a similar manner. The glass slides were cleaned with the pressurized air gun and IPA in addition to being left on a hotplate at 80 C to remove the IPA from the substrate surface before silver blade coating.

3.3. Silver electrode fabrication

For fabricating silver electrodes on the Kapton substrates, silicone release agent-free adhesive plastic tape (SPS, PN:1008R-6.0) was utilized as a mask. To support stronger adhesion to the Kapton substrates and ensure higher resolution, silver deposition isopropanol was used as a bonding agent between the Kapton substrate and silicon adhesive tape. Following this step, the edges of the silicon adhesive tape were sealed with masking tape. The masks were then laser cut using a Universal Laser Systems VLS 2.30 Desktop Laser Cutter and then wiped thoroughly with isopropanol to any unwanted debris remaining from laser cutting. For fabrication on glass slide substrates, the same silicone plastic tape was utilized with isopropanol as a binding agent. After the application of the tape to the substrate, the substrate was heated on a hotplate at 80 °C for 5 minutes, placed in the laser cutter for mask preparation, and the debris was removed with isopropanol. Prior to its application, the conducting silver nanoparticle paste (LS-453-6B, Asahi Chemical Research Laboratory Ltd, Japan) was homogeneously mixed to ensure the uniform dispersion of nanoparticles. This was achieved using a sterile swab to manually stir the paste, following which the mixture was immediately applied to one side of the electrode mask. A handheld metal (aluminium) blade squeegee was utilized to blade-coat the silver nanoparticle paste. This process facilitated a consistent application and optimal electrical conductivity of the resulting film. The paste underwent a thermal sintering process, which was carried out using a standard oven at 80 °C for a period of 60 minutes, adhering to the guidelines provided by the manufacturer.

3.4. Electroplating copper

To electrochemically deposit copper onto the silver blade-coated electrodes on Kapton and glass substrates, an electroplating electrolyte solution was prepared with copper(II) sulphate pentahydrate (Fluorochem UK) dissolved in 5% acetic acid (Chem-Lab NV). The concentrations of copper sulphate pentahydrate used in the experiments were 6.3 mM, 40 mM, and 100 mM. To set up the electroplating system, a coiled copper wire of 150 mm in length and 1 mm in diameter was utilized as the working electrode (anode), while the blade-coated silver electrode on the Kapton or glass substrate acted as the counter electrode (cathode). The silver blade-coated electrodes were cleaned thoroughly with DI water and dried with a pressurized air gun to remove any residual contaminants prior to electroplating, ensuring a clean surface for effective copper deposition. The electrodes were then positioned in the electroplating electrolyte such that the coiled copper wire was fully immersed and spaced evenly from the silver electrode to promote uniform copper plating. Electroplating was carried out by applying a constant chronoamperometric voltage of 1.5 V across the electrodes for a period of 20 minutes. This controlled application of voltage facilitated the migration of copper ions

towards the silver electrode, where they were reduced and deposited as a copper layer. Following the electroplating process, the electrodes were carefully removed from the solution and rinsed with distilled water and once again blown with a pressurized air gun to eliminate any excess copper sulphate from the surfaces.

Silver chloride coating on silver track (Ag/AgCl) was electrochemically deposited by using chronoamperometry (1.1 V) for 15 seconds, using 1 M hydrochloric acid (HCl) as the supporting electrolyte and solvent. The silver tracks of the FIDE were used as the anode while a sheet of platinum on a glass shaft electrode was set as the cathode.

3.5. Electrochemical gelation of PEDOT:PSS

For the electrochemical gelation of PEDOT:PSS onto silver–copper-plated electrodes, an aqueous solution consisting of 10 v/v% of PEDOT:PSS in deionized water was prepared and used as an electrolyte. The electrochemical cell setup involved using a single silver–copper-plated electrode as the working electrode, an electrode consisting of a thin sheet of platinum embedded into a glass shaft (Metrohm) as the counter electrode, and an Ag/AgCl reference electrode with a double-junction system (Metrohm) as the reference electrode. The electrochemical gelation process was initiated by immersing the silver–copper-plated electrode into the PEDOT:PSS solution, ensuring that it was positioned so that the reference electrode would be located centrally between the platinum counter electrode and the silver copper-plated electrode. The electrogelation was carried out at three different time intervals, 15 seconds, 90 seconds, and 500 seconds, to study the impact of gelation time on the properties of the films. Upon completion of the set gelation time, the electrode with the deposited PEDOT:PSS film was carefully extracted from the electrochemical cell. It was immediately rinsed thoroughly with DI water to remove any unbound or excess PEDOT:PSS from the surface. The electrogelated device was annealed at 100 °C for 5 minutes. After annealing, the electrode was allowed to cool down and dry at room temperature before use.

3.6. Atomic force microscopy (AFM) measurements

The surface roughness and morphology were studied using images recorded from AFM. A 5420 Agilent Technologies AFM was utilized in tapping mode, with a tip radius of 8 nm (Bruker FESP-V2) as the scan parameters. The samples were all processed using AFM on the glass slide substrates.

3.7. Scanning electron microscopy (SEM) measurements

The homogeneity of the electrode surfaces was analysed using SEM recordings that were collected under high vacuum ($< 4 \times 10^{-6}$ mbar) using the LEO GEMINI 1530VP FEG-SEM system which incorporated an Oxford instruments energy dispersive X-ray spectroscopy (EDX) detector, which performed EDX mapping with an acceleration voltage of 10 kV at a working distance of $\approx$8 mm. Images obtained were from SEM using an acceleration voltage of 3 kV at a working distance of $\approx$5 mm and an in-lens secondary electron detector. Images with magnification values of 1k, 5k, and 10k were collected.

3.8. Energy dispersive X-ray (EDX) measurements

The composition of the electrodes was determined using EDX. At least three different points were evaluated for each condition. In each point, the surface was analysed three times. SEM-EDX measurements were conducted using an LEO GEMINI 1530VP FEG-SEM.

3.9. Impedance measurements on-skin

The on-skin impedances of the electrodes attached to the participants' forearms were measured using electrochemical impedance spectroscopy (EIS). These measurements were taken with a 2-electrode setup, where the fabricated electrode (WE) was positioned on the inner part of the left forearm, and commercial Ag/AgCl electrodes served as the reference electrode (RE) and counter electrode (CE). The measurements were conducted at 60 Hz, which falls within the middle of the EMG signal range.

3.10. Body surface potential mapping (BSPM)

BSPM devices were composed of 16 electrodes (4 × 4 array) of 1.5 × 1.5 mm^2 electrodes. To interface the device with an electrophysiology recording system (Intan RHS Stim/Recording System), a flat 16-channel flexible printed circuit (FFC) wire was thermally bonded to the array *via* an anisotropic conducting film (ACF). Moreover, medical adhesives, as pressure-sensitive adhesives, were used to adhere more gently to the skin than other adhesive products and reduce the risk of medical adhesive-related skin injury. The adhesive layer plays a crucial role in the function of the device by insulating the conducting tracks, as well as providing safe and comfortable adhesion to the skin with sufficient conformability.

All electromyography (EMG) recording experiments were conducted with prior approval from the Ethics Committee of the Department of Engineering at the University of Cambridge (approval date: 6/9/2018, project identifier: IONBIKE). The participant consent was obtained before the sessions. The EMG data were obtained at a sampling rate of 30 kHz using an RHS stimulation and recording system from Intan Technologies. Prior to recording, the test sites were cleaned with a tissue moistened with ethanol to prepare the skin. The inner forearm and hand thumb regions were the regions selected for biopotential recordings for this work. A standard Ag/AgCl cutaneous electrode (MLA 1010B, ADInstruments) was applied at the elbow to serve as the voltage reference. The EMG signals were processed through a 50 Hz notch filter and a band-pass filter set between 10 Hz and 150 Hz. The signal-to-noise ratio (SNR) was determined by the root mean square (RMS) value of the voltage recorded during muscle activity, normalized by the number of samples, and divided by the RMS of the voltage when the forearm or thumb was at rest, also normalized by the number of samples. The signal-to-noise ratio was calculated

using the following equation:

$$\mathrm{SNR} = 20 \times \log_{10}\left(\frac{\mathrm{SNR}_{\mathrm{signal}}}{\mathrm{SNR}_{\mathrm{base}}}\right)$$

3.11. Small fibre stimulation

The stimulation of small muscle fibres was conducted using a Digimeter DS7A current stimulator, and a medical-grade current stimulator was used as an electrical nerve and muscle stimulator for humans in clinical research. The current stimulator enables the customization of different parameters to configure stimulation, such as current amplitude (up to 100 mA), pulse width, and a maximum voltage cap that can be limited with a supplied voltage of up to 400 V. The interdigitated electrode was developed during this work, or the FIDE was fabricated *via* silver nanoparticle paste screen printing (Printed Electronics Ltd). For the experiments conducted within this study, the FIDE was fixed centrally across the wrist, covering the region anatomically defined as the carpal area. The location was prepared by first removing any hair present on the surface of the skin and cleaned with an IPA wipe. Before any stimulation, the electrical risk was assessed and evaluated to prevent any potentially harmful stimulation. A combination of the current amplitude and pulse duration applied falls within the categorization of currents that cause perceptible stimulation but no muscle reactions and are capped to fall within this category using a stimulating tool (according to IEC 60479-1:2018).

3.12. Aqueous size exclusion chromatography (SEC)

The polymer's molar mass was analysed by SEC/MALS/RI. The equipment was composed of an LC20 pump (Shimadzu) coupled to a miniDawn Treos multiangle (3 angles) light scattering laser and an OptilabT—Rex differential refractometer (all from Wyatt Technology Corp., USA), using ultrahydrogel columns by Water. The analyses were carried out at 35 °C in water using 0.1 M NaCl at a flow rate of 0.6 mL min^{-1}.

3.13. Synthesis of poly (styrene sulphonate-*co*-styrene methanamine) (PSS-*co*-PSMA)

2 g of sodium 4-vinylbenzenesulphonate in 25 mL of MilliQ water and 0.5 g of (4-vinylphenyl)methanamine hydrochloride were added to a 50 mL round bottom flask equipped with a magnetic stirring bar. Then, AIBA (0.25 g, 10 wt%) was added and the oxygen was eliminated by bubbling argon while stirring for 1 h. Then, the flask was placed and stirred at 70 °C for 18 h under an inert atmosphere using an argon balloon. The work up of the solution was achieved by precipitating it in an excess (250 mL) of methanol, filtering using a Büchner funnel and drying under vacuum. The polymer was characterized using ^{1}H-NMR spectroscopy (Fig. S5, ESI†) and GPC (Fig. S6, ESI†)

3.14. Synthesis of PEDOT:PSS-*co*-PSMA

PEDOT:PSS-*co*-PSMA was synthesized following previous reports[38] to mimic the commercialized solution. In a 250 mL reactor filled with 100 mL of deionized (DI) water, 1.42 g of PSS-*co*-PSMA was added and stirred at 600 rpm for 30 min at r.t. until a clear solution is formed. 0.572 g of EDOT was added and after 15 min at r.t., 1.5 eq. (with respect to EDOT, 0.919 g) of $(NH_4)_2S_2O_8$ and a catalytic amount of $Fe_2(SO_4)_3$ were added. This led to dispersions of 2% solid content and a relationship between PEDOT and an anionic stabilizer of 1 : 2.5 in mass. The dispersion was stirred until complete conversion, usually for 24 h. Finally, the dispersion was dialyzed in MilliQ for 2 days using a MWCO membrane of 14 kDa.

4. Conclusions

In summary, in this work, we have developed a lithography-free technique to make coatings of PEDOT:PSS on silver electrodes using electrogelation as an alternative method to electropolymerisation. The resulting electrodes show potential for high-resolution electrophysiological recordings and stimulation, as well as potential applications in biosensing and organic electronic devices. Indeed, PEDOT:PSS-coated electrodes demonstrated significantly lower voltage parameters to reach the same stimulating current, as well as improved signal-to-noise ratio (SNR) for biopotential recordings, particularly with lower (6.3 mM) and medium (40 mM) concentrations of $CuSO_4$ used in the electrogelation process, respectively. Furthermore, the electrogelation technique provides a scalable and cost-effective solution for the deposition of conventional conducting polymers (PEDOT:PSS) and non-solution processable new synthesis of PEDOT:PSS-based copolymers such as PEDOT:PSS-*co*-PSMA. PEDOT:PSS-*co*-PSMA was integrated as the gate electrode in an OECT, showing better performance than the non-modified gold electrode and its PEDOT:PSS counterpart. This approach is pivotal for advancing the development of functional bioelectronic devices and has significant potential for applications in emerging fields, such as thermoelectric devices where non-noble metals are required. All in all, we believe that this work explores in detail the technique of electrogelation and offers a set of fundamental examples for its use in bioelectronics-related fields.

Data availability

The data supporting this article have been included as part of the ESI.†

Conflicts of interest

There are no conflicts to declare.

Acknowledgements

C. S. acknowledges financial support from the Gates-Cambridge Trust. S. T. K. gratefully acknowledges funding from the European Union's Horizon 2020 research and innovation programme under the Marie Skłodowska-Curie grant agreement 101022365. S. T. K. and G. G. M. acknowledge support from the Engineering and

Physical Sciences Research Council (UK) (Grant EP/W017091/1). GM and AD-A acknowledge the financial support from the EU (COPE-Nano, ID: 101059828) and EPSRC IRC in Targeted Delivery for Hard-to-Treat Cancers (EP/S009000/1). RM acknowledges the EPSRC CDT in Nanoscience and Nanotechnology (EP/L015978/1). S. V.-B acknowledges funding from the W. D. Armstrong Studentship. R. R.-M. S. acknowledges the EPSRC grant (EP/S022139/1).

References

1 A. Ruggiero, V. Criscuolo, S. Grasselli, U. Bruno, C. Ausilio, C. L. Bovio, O. Bettucci and F. Santoro, *Chem. Commun.*, 2022, **58**, 9790–9793.
2 J.-C. Hsieh, Y. Li, H. Wang, M. Perz, Q. Tang, K. W. K. Tang, I. Pyatnitskiy, R. Reyes, H. Ding and H. Wang, *J. Mater. Chem. B*, 2022, **10**, 7260–7280.
3 F. Bonafè, F. Decataldo, T. Cramer and B. Fraboni, *Adv. Sci.*, 2024, **11**, 2308746.
4 J. Abu Shihada, M. Jung, S. Decke, L. Koschinski, S. Musall, V. Rincón Montes and A. Offenhäusser, *Adv. Sci.*, 2024, **11**, 2305944.
5 C. Bodart, N. Rossetti, J. Hagler, P. Chevreau, D. Chhin, F. Soavi, S. B. Schougaard, F. Amzica and F. Cicoira, *ACS Appl. Mater. Interfaces*, 2019, **11**, 17226–17233.
6 N. Rossetti, J. Hagler, P. Kateb and F. Cicoira, *J. Mater. Chem. C*, 2021, **9**, 7243–7263.
7 N. Rossetti, P. Luthra, J. Hagler, A. H. Jae Lee, C. Bodart, X. Li, G. Ducharme, F. Soavi, B. Amilhon and F. Cicoira, *ACS Appl. Bio Mater.*, 2019, **2**, 5154–5163.
8 J. Hagler, J. Yeu, X. Zhou, G. Ducharme, B. Amilhon and F. Cicoira, *Adv. Mater. Interfaces*, 2022, **9**, 2201066.
9 A. Güemes, A. Dominguez-Alfaro, R. Mizuta, S. Velasco-Bosom, A. Carnicer-Lombarte, D. G. Barone, D. Mecerreyes and G. Malliaras, *Mater. Adv.*, 2023, **4**, 6741–6753.
10 G. G. Leisk, T. J. Lo, T. Yucel, Q. Lu and D. L. Kaplan, *Adv. Mater.*, 2010, **22**, 711–715.
11 N. Kojic, M. J. Panzer, G. G. Leisk, W. K. Raja, M. Kojic and D. L. Kaplan, *Soft Matter*, 2012, **8**, 6897–6905.
12 V. R. Feig, H. Tran, M. Lee, K. Liu, Z. Huang, L. Beker, D. G. Mackanic and Z. Bao, *Adv. Mater.*, 2019, **31**, 1902869.
13 H. He, R. Chen, S. Yue, S. Yu, J. Wei and J. Ouyang, *Sci. Adv.*, 2024, **8**, eabq8160.
14 Q. Gao, P. Wang, M. Wang, Y. Wang and J. Zhu, *Compos. Commun.*, 2021, **25**, 100700.
15 D. Xu, X. Feng, D. Niu, X. Zhu and Y. Song, *Mater. Today Commun.*, 2020, **24**, 101090.
16 C. Yu, C. Wang, X. Liu, X. Jia, S. Naficy, K. Shu, M. Forsyth and G. G. Wallace, *Adv. Mater.*, 2016, **28**, 9349–9355.
17 M. A. Leaf and M. Muthukumar, *Macromolecules*, 2016, **49**(11), 4286–4294.
18 V. R. Feig, H. Tran, M. Lee and Z. Bao, *Nat. Commun.*, 2018, **9**, 2740.
19 A. Aguzin, A. Dominguez-Alfaro, M. Criado-Gonzalez, S. Velasco-Bosom, M. L. Picchio, N. Casado, E. Mitoudi-Vagourdi, R. J. Minari, G. G. Malliaras and D. Mecerreyes, *Mater. Horiz.*, 2023, **10**, 2516–2524.
20 T. Li, Z. Ye, Y. Cai, T. Tu, B. Zhang, S. Zhang, L. Fang, X. Mao, S. Xu, X. Ye and B. Liang, *J. Electroanal. Chem.*, 2022, **911**, 116183.
21 Y. Cai, T. Tu, T. Li, S. Zhang, B. Zhang, L. Fang, X. Ye and B. Liang, *J. Electroanal. Chem.*, 2022, **922**, 116738.
22 Y. Deng, T. Shang, Z. Wu, Y. Tao, C. Luo, J. Liang, D. Han, R. Lyu, C. Qi, W. Lv, F. Kang and Q.-H. Yang, *Adv. Mater.*, 2019, **31**, 1902432.
23 S. Zhang, T. Tu, T. Li, Y. Cai, Z. Wang, Y. Zhou, D. Wang, L. Fang, X. Ye and B. Liang, *ACS Appl. Mater. Interfaces*, 2022, **14**, 23877–23887.
24 T. Tu, B. Liang, S. Zhang, T. Li, B. Zhang, S. Xu, X. Mao, Y. Cai, L. Fang and X. Ye, *Adv. Funct. Mater.*, 2021, **31**, 2101374.
25 M. Monfared Dehbali, M. Farahmandpour, S. Hamedi and Z. Kordrostami, *Sci. Rep.*, 2023, **13**, 9505.
26 S. Velasco-Bosom, N. Karam, A. Carnicer-Lombarte, J. Gurke, N. Casado, L. C. Tomé, D. Mecerreyes and G. G. Malliaras, *Adv. Healthcare Mater.*, 2021, **10**, 2100374.
27 R. R.-M. Serrano, S. Velasco-Bosom, A. Dominguez-Alfaro, M. L. Picchio, D. Mantione, D. Mecerreyes and G. G. Malliaras, *Adv. Sci.*, 2023, 2301176.
28 N. Casado, S. Zendegi, L. C. Tomé, S. Velasco-Bosom, A. Aguzin, M. Picchio, M. Criado-Gonzalez, G. G. Malliaras, M. Forsyth and D. Mecerreyes, *J. Mater. Chem. C*, 2022, **10**, 15186–15193.
29 H. Yabu, K. Nagamine, J. Kamei, Y. Saito, T. Okabe, T. Shimazaki and M. Nishizawa, *RSC Adv.*, 2015, **5**, 88414–88418.
30 Y. Liu, Y. Han, Z. Zhang, W. Zhang, W. Lai, Y. Wang and R. Cao, *Chem. Sci.*, 2019, **10**, 2613–2622.
31 S. Velasco-Bosom, J. Gurke, S. Han, M. C. Lee and G. G. Malliaras, *Adv. Mater. Technol.*, 2023, **8**, 2200748.
32 M. S. Lee, A. Paul, Y. Xu, W. D. Hairston and G. Cauwenberghs, *Front. Electron.*, 2022, **2**, DOI: **10.3389/felec.2021.700363**.
33 S. T. M. Tan, G. Lee, I. Denti, G. LeCroy, K. Rozylowicz, A. Marks, S. Griggs, I. McCulloch, A. Giovannitti and A. Salleo, *Adv. Mater.*, 2022, **34**, 2202359.
34 S. E. Doris, A. Pierre and R. A. Street, *Adv. Mater.*, 2018, **30**, 1706757.
35 L. Kergoat, L. Herlogsson, B. Piro, M. C. Pham, G. Horowitz, X. Crispin and M. Berggren, *Proc. Natl. Acad. Sci.*, 2012, **109**, 8394–8399.
36 S. T. Keene, T. P. A. van der Pol, D. Zakhidov, C. H. L. Weijtens, R. A. J. Janssen, A. Salleo and Y. van de Burgt, *Adv. Mater.*, 2020, **32**, 2000270.
37 T. P. A. van der Pol, S. T. Keene, B. W. H. Saes, S. C. J. Meskers, A. Salleo, Y. van de Burgt and R. A. J. Janssen, *J. Phys. Chem. C*, 2019, **123**, 24328–24337.
38 D. Mantione, I. del Agua, W. Schaafsma, J. Diez-Garcia, B. Castro, H. Sardon and D. Mecerreyes, *Macromol. Biosci.*, 2016, **16**, 1227–1238.

